BNL-224087-2023-TECH

EIC-ADD-TN-039

Time-domain simulation of the crab cavity/beam interaction

T. Mastoridis, K. Smith

February 2023

Electron-Ion Collider

Brookhaven National Laboratory

U.S. Department of Energy

USDOE Office of Science (SC), Nuclear Physics (NP) (SC-26)

DISCLAIMER

EIC TECHNICAL NOTE	NUMBER **EIC-ADD-TN-039**
AUTHORS: T. Mastoridis, T. Hidalgo, T. Loe, M. Toivola (California Polytechnic State University), K. Smith (BNL)	DATE 02/17/2023
Time-Domain Simulation of the Crab Cavity/Beam Interaction	

Abstract

The Electron-Ion Collider (EIC) will employ crab cavities to maximize luminosity. A time-domain simulation is developed to study the interaction between the particle beam and the crab cavities in the EIC, including the Low-Level RF (LLRF) feedback loops. The simulation is validated through power and induced voltage estimates. We then use the simulation tool to study the beam loading effects on the crabbing voltage and thus on the beam transverse position and tilt. We also study the crabbing voltage regulation and transmitter power transients as a function of the LLRF design.

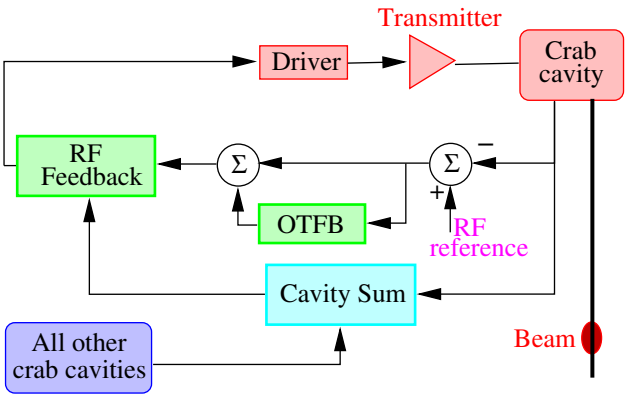

Figure 1: Crab Cavity RF/LLRF Block Diagram.

1 Simulation Description

The note showcases the Full Scope 10 GeV Electron Storage Ring (ESR) Crab Cavity system [1], with 18 Focusing accelerating cavities. In addition, all energy cases for both the ESR and the Hadron Storage Ring (HSR) were studied, and the results for all other cases, as well as the relevant crab cavity parameters, are summarized in Appendix A.

The time-domain simulation has block models representing the crab cavities, the transmitter, and the LLRF system loops. Each bunch is modeled as a single macroparticle. Each macroparticle includes the total bunch charge, the horizontal position of the bunch centroid, and longitudinal position of the bunch centroid. The ring beam pattern is replicated exactly (i.e. the number of macrobunches is equal to the number of planned bunches in the EIC) to achieve an accurate representation of the gap transient system behavior.

The Crab Cavity LLRF is under design. There are three important considerations:

- Transient beam loading effects on transverse beam position and transmitter power, described in this note.
- Minimizing the RF noise sampled by the beam to reduce transverse emittance growth. The corresponding studies can be found in [2].
- Impedance reduction/Transverse instability control: this issue has been presented in [3]. This study needs to be translated to LLRF specifications.

Figure 1 shows a block diagram of the Crab Cavity RF/LLRF. The RF feedback includes a narrowband integrator to regulate the mean value of the cavity voltage, as well as a proportional controller. This work studies the controller around individual stations, but, as the block diagram indicates, it might eventually be useful to add an additional controller that keeps the total crabbing and uncrabbing voltage to zero. Such a system would sample the Cavity Sum signal and act on one or all cavities to keep the sum to zero. We refer to this system as the "global" controller. In addition, a One-Turn Feedback system (OTFB) at the betatron sidebands of the revolution harmonics could be added in the future if the transverse instabilities study indicates that additional impedance control is required.

We validate the simulation by comparing results with analytical expressions for the transmitter power as a function of various operational parameters and the beam-induced voltage in the crab cavities. The validation study is summarized in Appendix B.

2 Transient Beam Loading Effects

The simulation is first used to study transient beam loading effects. These metrics include the transverse offset at the Interaction Point (Δx_{IP}), the transverse offset *after* uncrabbing ($\Delta x_{\mathrm{offset}}$, due to transients *and* the crabbing/uncrabbing asymmetry), and the transmitter power transients.

The re-scaled crab cavity transmitter current is given by [4]:

$$J_g = \left[\frac{V_\perp}{2(R/Q)_\perp}\frac{1}{Q_L} + \frac{x\omega}{c} I_{b,DC} F_b sin(\phi_b)\right] + i\left[\frac{x\omega}{c} I_{b,DC} F_b cos(\phi_b) - \frac{V_\perp \Delta\omega}{\omega(R/Q)_\perp}\right] \quad (1)$$

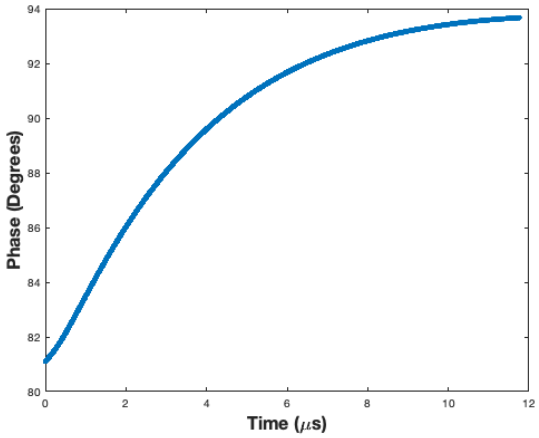

Figure 2: Bunch phase over a turn.

with $V_\perp$ the crab cavity voltage, $(R/Q)_\perp$ is the crab cavity's transverse R/Q value, Q_L the crab cavity loaded quality factor, x the transverse bunch position, ω the crab cavity angular RF frequency, c the speed of light, $I_{b,DC}$ the DC beam current, F_b the bunching factor, ϕ_b the beam synchronous phase, and $\Delta\omega$ the crab cavity detuning.

From the above equation, we see that in order to have *any* induced voltage, we need to assume a transverse bunch position error (x_{error}) going into the crab cavities. We investigated the case of a constant 0.6 mm offset (the alignment specification within the cryostat) and random errors of 1, 10, and 100 μm rms. The 1 μm case is probably close to what could be achieved by a transverse feedback system. We also assumed zero detuning.

In addition, it is necessary to model transient beam loading in the *accelerating* cavities so that ϕ_b is different than zero and the crab cavity induced voltage has an imaginary component (proportional to $cos(\phi_b)$). The stable phase ϕ_b for all bunches is extracted from a time-domain simulation of the EIC accelerating system [5], as shown in Figure 2. We assume a phase loop will keep the *mean* bunch phase over a turn synchronized with the RF reference. As a result, the beam phase experienced by the crab cavities will have a mean of ninety degrees.

2.1 Constant x_{error}

We first investigated the case of a constant transverse bunch position error ($x_{error} = 0.6$ mm). The Δx_{IP} and Δx_{offset} transients are shown for three different LLRF gains in Figures 3, 4. The gains are set for 7, 10, and 13 dB margins. Clearly from the figures, the transient beam loading in the crab cavities leads to *very* small effects on Δx_{IP} and Δx_{offset} (note the vertical scale in μm and nm respectively), even with a low LLRF gain/bandwidth. Therefore the gain requirements will most likely be set by impedance control and transverse instability reduction requirements [3].

The associated induced voltage in the crabbing and uncrabbing cavities is shown in Figures 5, 6. Again, it is a minimal effect on the order of kV (compared to the 1.08 MV cavity reference voltage). The effect on crabbing/uncrabbing voltage is *almost* perfectly symmetric: the x-offset introduced by the crabbing voltage transient *slightly* changes the induced voltage in the uncrabbing cavity.

Transient beam loading significantly affects the transmitter power transients, as shown in Figures 7, 8. Depending on the LLRF gain/bandwidth choices, the peak power can be *double* the average or analytically computed power. This increase is not concerning but should be included in the transmitter specifications. A low LLRF gain leads to a lower closed loop bandwidth, which filters the gap transient and significantly reduces the power transients. We should also note the significant power difference between crabbing and uncrabbing transmitters since the power is added to and extracted from the beam respectively. The situation would be reversed for a *negative* x_{error}. The value P_{batch} is analytically computed from Equation 5 and corresponds to the power due to the peak beam current, as described in Appendix C.

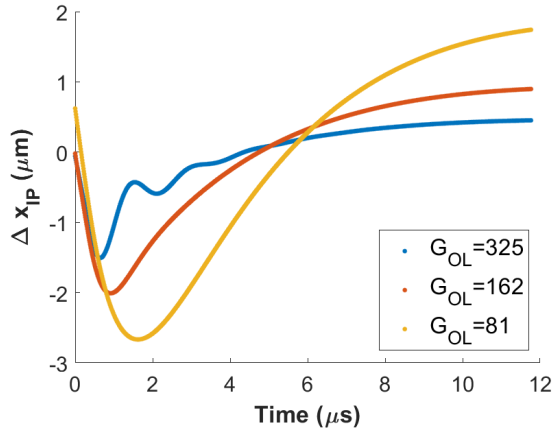

Figure 3: x-offset at the IP.

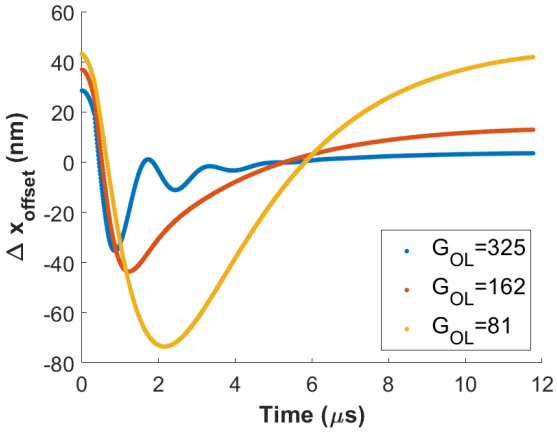

Figure 4: Residual x-offset after uncrabbing.

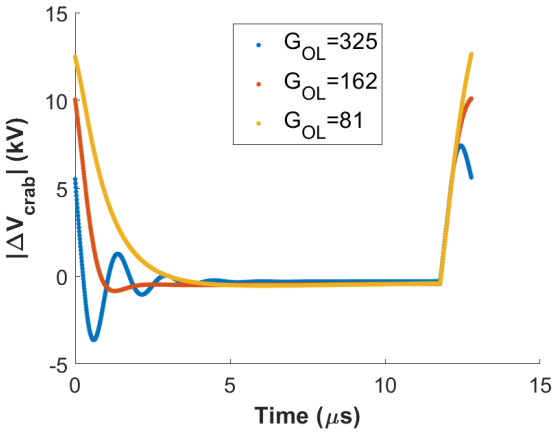

Figure 5: Transient beam loading on 1.08 MV crabbing voltage.

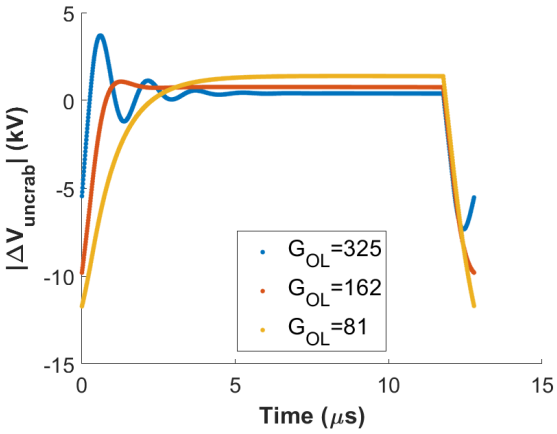

Figure 6: Transient beam loading on 1.08 MV uncrabbing voltage.

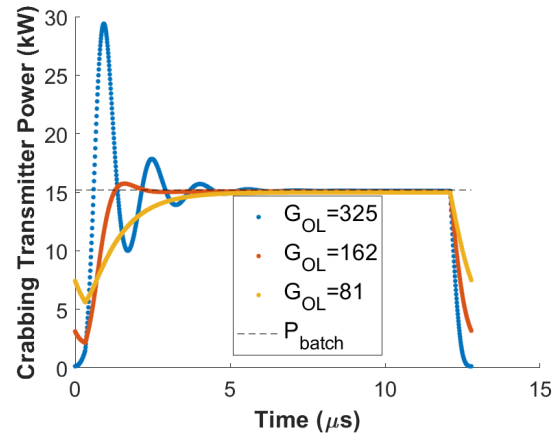

Figure 7: Crabbing transmitter power.

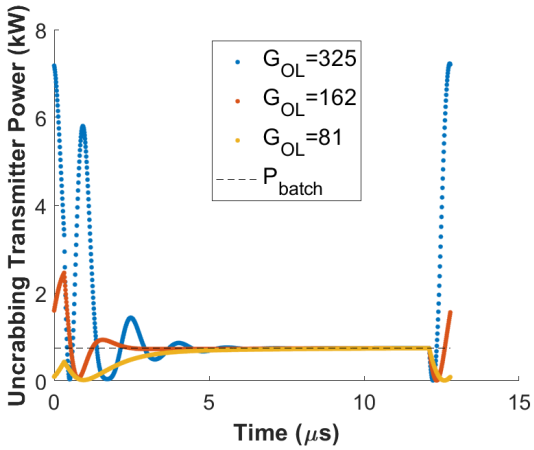

Figure 8: Uncrabbing transmitter power.

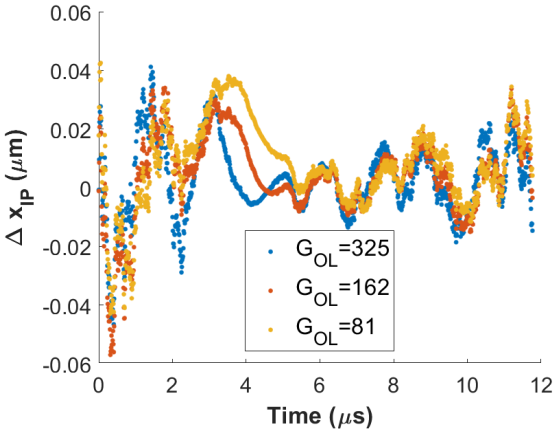

Figure 9: x-offset at the IP.

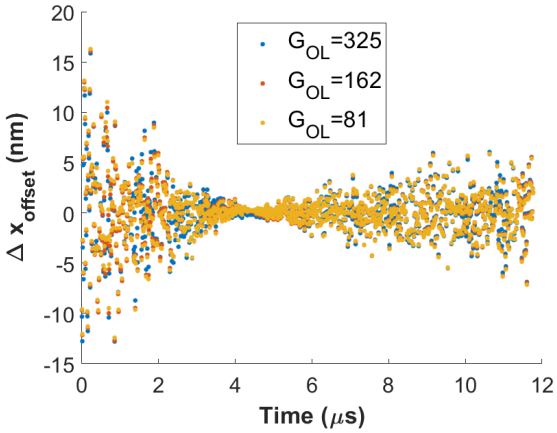

Figure 10: Residual x-offset after uncrabbing.

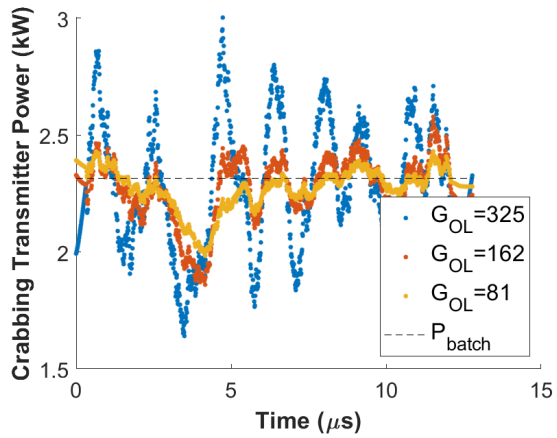

Figure 11: Crabbing transmitter power.

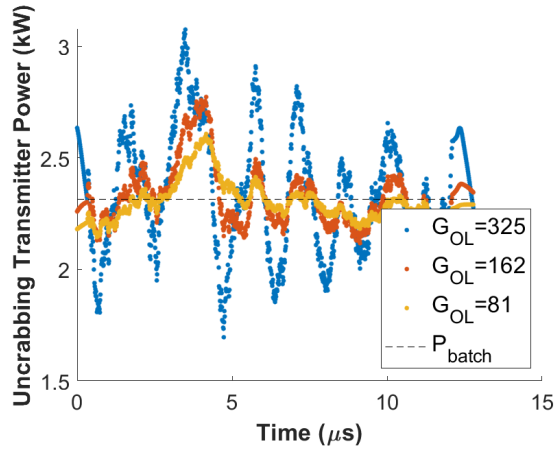

Figure 12: Uncrabbing transmitter power.

2.2 Random x_{error}

We then investigate a random transverse bunch position error and present the results for the case of 100 μm rms. In the machine, an rms on the order of 1 μm is realistic, so this is an especially conservative case. The effect due to this random error on the bunch transverse position is still insignificant, as shown in Figures 9, 10. The induced voltage is also minimal. As expected, the results for 1 or 10 μm rms are similarly not concerning.

The peak power is much higher than the analytically estimated value, similar to the constant x_{error} case (Figures 11, 12). This power transient is small though, and is not significant compared to the power due to a constant x_{error}. So, for practical purposes, only the constant case needs to be considered for transmitter power specifications.

3 Loop Delay Effects

We also used the simulation tool to investigate the dependence of transient beam loading effects on the LLRF delay. We used x_{error} =0.6 mm for this study, since the rms noise case does not produce significant transient beam loading effects.

The LLRF gain is lowered to maintain a 10 dB margin with a higher delay of 640 ns. The actual gain is comparable to the 13 dB margin case with the nominal 320 ns delay. Since the delay dominates the phase rotation, a two-fold increase in delay requires a reduction of the gain by a factor of 2 (3 dB) to maintain the same gain margin.

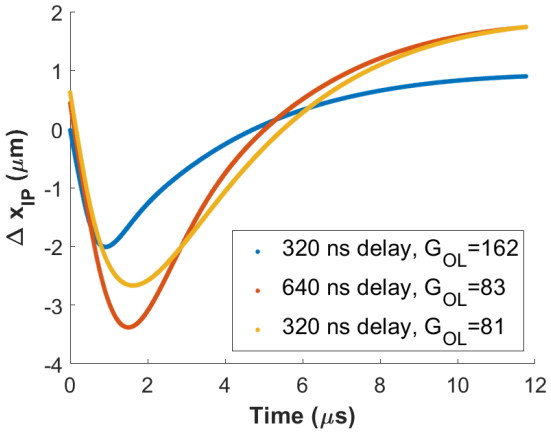

Figure 13: x-offset at the IP.

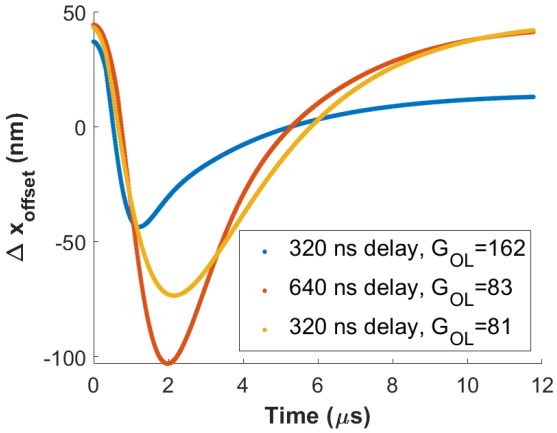

Figure 14: Residual x-offset after uncrabbing.

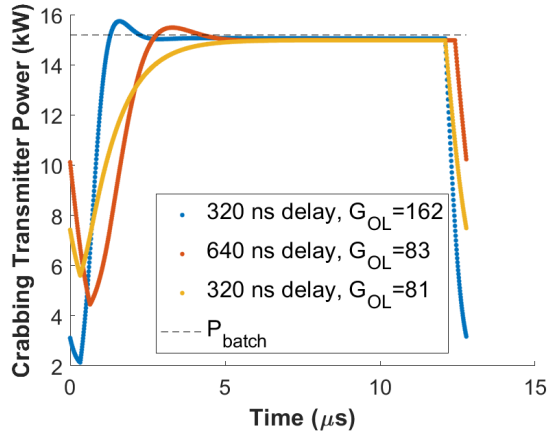

Figure 15: Crabbing transmitter power.

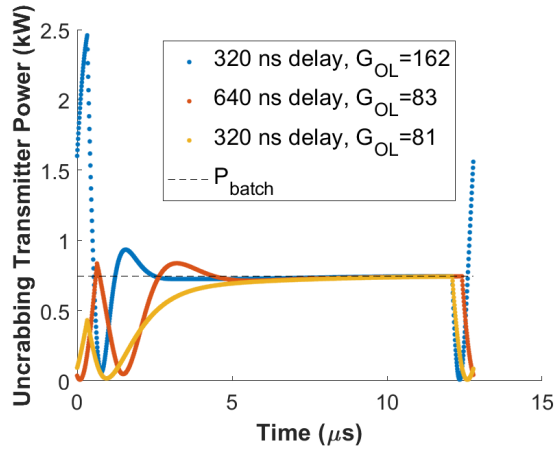

Figure 16: Uncrabbing transmitter power.

Unsurprisingly, there are minor differences in the beam's transverse position, given the very high Q_L and the very small effects observed so far, as shown in Figures 13, 14. The high delay case resembles the 13 dB gain margin case due to its similar gain setting.

The loop delay effect is more noticeable on the transmitter power. The power transients are *lower* with the higher delay setting since the gain is lower to maintain the 10 dB gain margin, as seen in Figures 15, 16.

The results from the delay study suggest that we could consider the possibility of deliberately lowering the LLRF gain to achieve lower peak transient power with minimal effect on beam performance. However, there is a significant tradeoff with impedance reduction, so the viability of this choice must be checked against the requirements for transverse instability control.

4 One-Turn Feedback (OTFB)

A One-turn Feedback (OTFB) system will most likely be required for impedance control [3]. This system will supplement the RF Feedback as shown in Figure 1. A simplified diagram of the OTFB is shown in Figure 17. It will act at the betatron sidebands of the revolution harmonics to further reduce the impedance (H_{OTFB} in Figure 17). The width of the peaks at the betatron sidebands should be higher than the tune spread. A tradeoff exists between the peak width and OTFB gain, which is currently set to 10. The OTFB path will also include a low-pass filter, with a bandwidth wider than the closed-loop cavity bandwidth. The bandwidth choice is further explored in

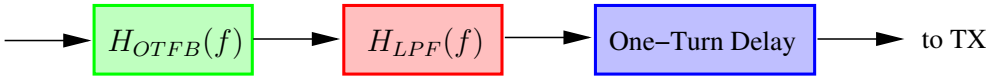

Figure 17: OTFB Block Diagram.

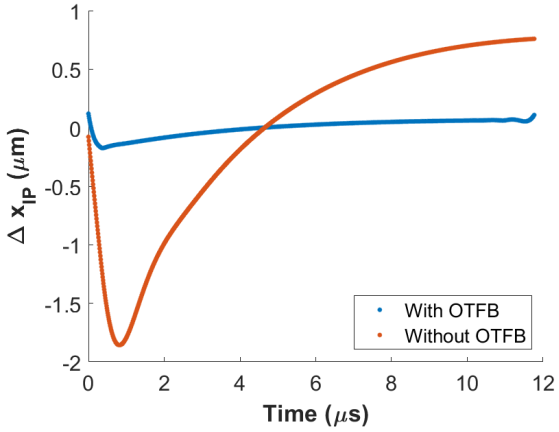

Figure 18: x-offset at the IP.

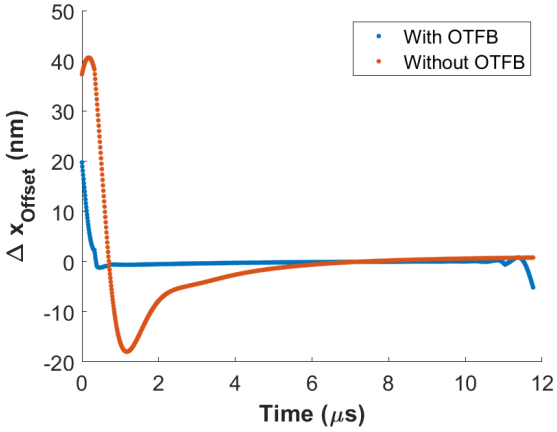

Figure 19: Residual x-offset after uncrabbing.

Appendix D. Finally, the OTFB path includes a delay to make the total OTFB delay *almost* equal to the revolution period. The slight offset maximizes the loop stability by increasing the phase margins at the non-linear part of the phase response [6].

Figures 18 and 19 show the performance improvement with the OTFB. The peak to peak x-offset at the IP is reduced by a factor of about 9 (from 2.6 to 0.29 μm). The rms value is similarly reduced from 740 to 65 nm (factor of 11). This is inline with the OTFB gain setting of 10.

The transmitter power is minimally affected in the presence of the OTFB, as shown in Figures 20 and 21.

5 Global Controller

The main function of the global controller will be to ramp the crabbing/uncrabbing cavities down in case of a station loss, due to a quench, transmitter trip, RF/LLRF fault etc. The goal is to minimize the effects on the beam

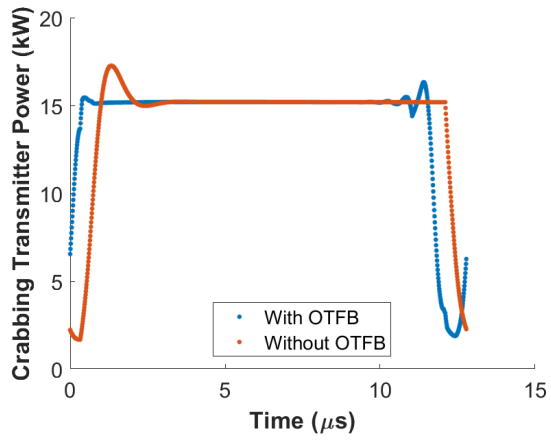

Figure 20: Crabbing transmitter power.

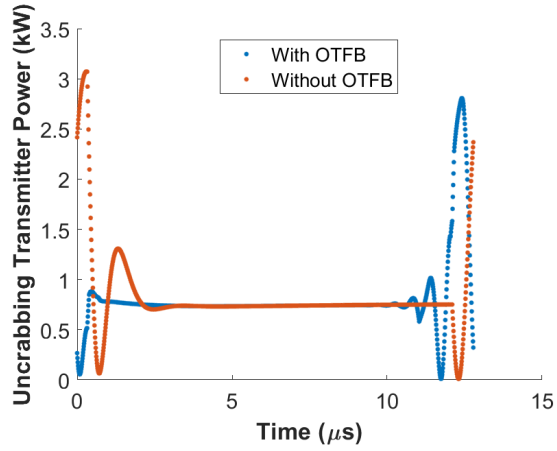

Figure 21: Uncrabbing transmitter power.

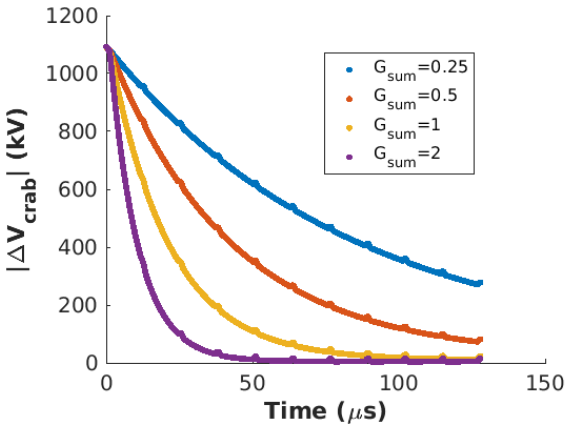

Figure 22: Crabbing cavity voltage (10 turns).

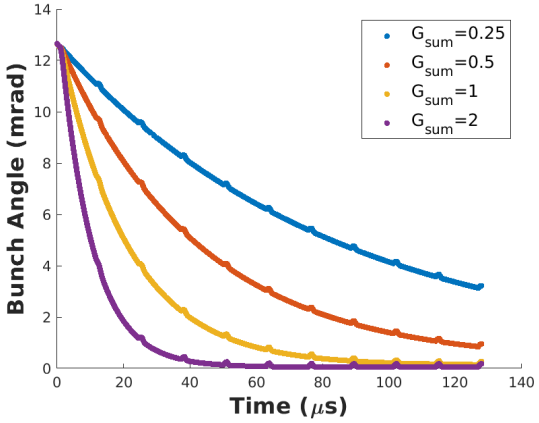

Figure 23: Additional bunch-by-bunch rotation per turn (10 turns).

and thus the danger on accelerator structures for the few turns before an interlock is activated and the beam is dumped. The global controller calculates the cavity sum, which should ideally be zero. When a crabbing station is lost, the controller reduces the voltage of the uncrabbing stations accordingly. If an uncrabbing station is lost, it acts on the crabbing cavities. The global controller is modelled as a low-gain integrator.

Figures 22-24 show the crabbing voltage, the resulting residual bunch-by-bunch x-offset and bunch tilt, and the transmitter power for the first few turns after a trip of an uncrabbing cavity. Table 1 shows the important values from these plots for each case.

Gain	Time to $\frac{1}{e}V_o$ (turns)	Peak Power (kW)	Worst-case tilt (mrad)	Maximum x_{IP} deviation (μm)
0.25	3.48	9.33	97.9	2.49
0.5	7.07	9.49	146	2.24
1	1.73	15.3	59.9	2.11
2	0.860	137	38.8	2.05
3	0.619	381	32.4	2.04

Table 1: Comparison of global controller performance metrics

There is a tradeoff between the global controller response time and the required transmitter power. As seen in Figures 22 and 25, increasing the controller gain to leads to a significant increase in the required power. The controller is tasked with reducing the voltage to zero within a couple of terms. This is effectively equivalent to *filling* the cavity to the nominal field, and thus requires significant power.

Unrealistic power levels would be required to further reduce the response time to a fraction of a turn. With the realistic gains shown in Figures 22-24, the bunch-by-bunch x-offset is very small and should not be of concern. The *additional* bunch-by-bunch rotation per turn gets quickly reduced after the first turn. Since this simulation does not include particle tracking, it is not possible to accurately estimate the *accumulated* bunch rotation. Given the non-integer tune though, it should not be any higher than the rotation at the first turn, which is comparable to the half-crabbing angle for the first few bunches and is slowly reduced thereafter.

The optimal gain for the global controller can be selected once the transmitter peak power is specified.

6 Conclusions and Future steps

We developed a simulation of the beam-crab cavity LLRF/RF interaction to study crab cavity transient beam loading effects on transverse position and transmitter power. There are generally negligible effects on the transverse position. The peak transmitter power deviates somewhat from the analytical expressions, and, while not concerning, should still be taken into consideration when specifying the transmitters.

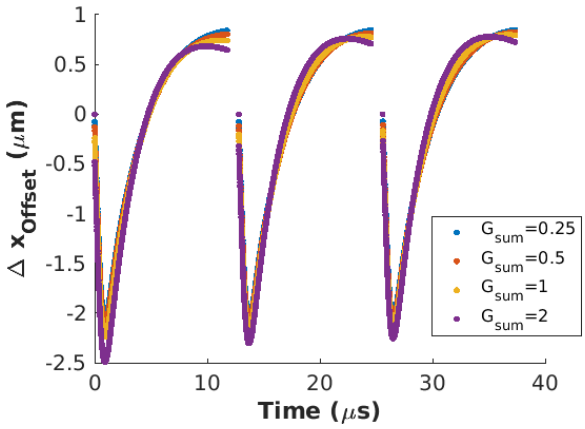

Figure 24: x-offset after passing the uncrabbing cavity (3 turns).

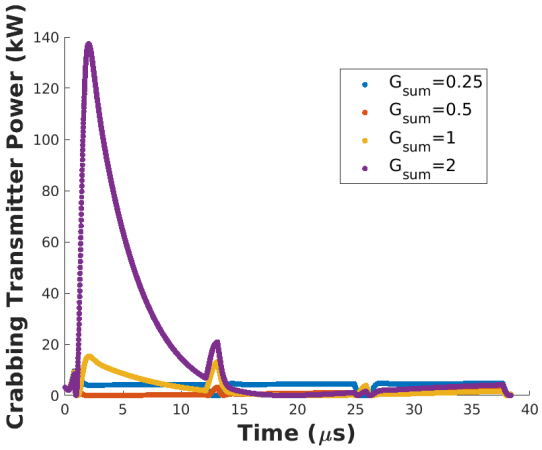

Figure 25: Crabbing transmitter power (3 turns).

A OTFB system was also studied. It will significantly reduce transient beam loading effects, with minimal to no cost on transmitter power.

A global controller was introduced, to simulate the ramping down of the crabbing/uncrabbing voltage in case of a station loss. The transient effects on bunch position and rotation do not seem concerning.

As the design matures, this tool will be valuable for future crab cavity LLRF studies. We plan to use this simulation to investigate feedback control of the cavity voltage sum (the LLRF should regulate individual station voltages and the total crabbing/uncrabbing voltage). This study will investigate the effectiveness of narrowband systems at individual stations, with one global wideband control of the total crabbing/uncrabbing voltage. In theory, such an architecture would reduce the total RF noise sampled by the beam. However, it might be necessary to design the opposite for impedance control (wideband local systems with a narrowband global controller). This architecture will be investigated as well.

Finally, tradeoffs likely exist between low noise and high impedance control architectures. We can use this simulation tool to evaluate these tradeoffs.

References

[1] F. Willeke and J. Beebe-Wang, "Electron ion collider conceptual design report 2021," Feb. 2021.

[2] K. Smith, T. Mastoridis, P. Fuller, P. Mahri, and Y. Matsumura, "Eic transverse emittance growth due to crab cavity rf noise: Estimates and mitigation," Feb. 2022.

[3] M. Blaskiewicz, "Instabilities driven by the fundamental crabbing mode," Oct. 2021.

[4] J. Tückmantel, "Cavity-Beam-Transmitter Interaction Formula Collection with Derivation," Tech. Rep. CERN-ATS-Note-2011-002 TECH, Oct. 2010.

[5] T. Mastoridis, J. D. Fox, J. Guo, R. A. Rimmer, and H. Wang, "Beam gap transient analysis and mitigations in high-current storage rings for an electron-ion collider," *Phys. Rev. Accel. Beams*, vol. 23, p. 101601, Oct 2020.

[6] P. Baudrenghien, T. Mastoridis, and J. Molendijk, "The LHC One-Turn Feedback," 2012.

A Crab Cavity parameters and results for all energy cases

The crab cavity parameters used in this study and the results for all energy cases are summarized in Table 2. N_p is the number of particle per bunch.

Energy Case	V_{cav} (MV)	N_{cav}	$(R/Q)_\perp$	Q_{loaded}	N_p
ESR 5GeV	0.58	1	315	1.08×10^5	1.72×10^{11}
ESR 10GeV	1.08	1	315	2×10^5	1.72×10^{11}
ESR 18GeV	2.55	1	315	1×10^6	0.62×10^{11}
HSR 41GeV	2.02	4	1160	1×10^6	0.26×10^{11}
HSR 100GeV	3.57	4	1160	1×10^6	0.69×10^{11}
HSR 275GeV	6.09	4	1160	1×10^6	1.91×10^{11}

Table 2: Simulation parameters for all energy cases.

Energy Case	ΔX_{IP} (Pk-Pk, μm)	ΔX_{offset} (Pk-Pk, nm)
ESR 5GeV	14.5	717
ESR 10GeV	2.91	80.6
ESR 18GeV	0.00209	0.121
HSR 41GeV	1.57	24.6
HSR 100GeV	0.790	9.05
HSR 275GeV	0.281	11.6

Table 3: Transverse offsets for all energy cases.

Energy Case	Analytical P_{Crab} (kW)	Peak P_{Crab} (kW)	Analytical P_{Uncrab} (kW)	Peak P_{Uncrab} (kW)
ESR 5GeV	7.40	8.25	0.286	1.31
ESR 10GeV	13.8	15.7	0.471	2.46
ESR 18GeV	4.20	4.41	1.35	2.60
HSR 41GeV	1.36	1.40	0.0270	0.454
HSR 100GeV	6.66	6.95	0.0580	1.44
HSR 275GeV	9.46	9.72	0.845	4.04

Table 4: Transmitter power for all energy cases.

As shown in Section 2, the transient beam loading effects due to random transverse position errors are insignificant compared to the constant x_{error} case. As a result, Tables 3 and 4, summarize the results for all energy cases assuming a constant x_{error} of 0.6 mm. In addition, the results correspond to a LLRF gain setting that achieves a 10 dB gain margin. As shown in Section 2, a higher gain is found to slightly reduce transient beam loading effects but with an increase in power transients. Similarly, a lower gain would slightly reduce beam performance and slightly lower power transients. These small variations do not change the general conclusions from Tables 3 and 4.

From these tables, we conclude that the transverse position offsets are insignificant for all cases. The transmitter power transients, while not concerning, are higher than the analytically estimated values, which should be taken into consideration for transmitter specification. Finally, the 5 GeV case has the highest transients. This is to be expected since the beam current is the same as the 10 GeV case while the cavity voltage is the lowest of all cases; a much higher ratio of induced voltage to reference voltage (higher beam loading). Still, the transverse offsets are practically negligible, and the power transients are not concerning.

B Simulation validation

The simulation is validated *in steady state* by comparing simulation results with analytical expressions for the transmitter power as a function of various operational parameters (Q_L and transverse bunch position error x_{error}),

as well as by checking the optimal Q_L for minimal transmitter power. The optimal transmitter power is given by [4]:

$$P_g(x) = \frac{1}{2}(R/Q)_\perp Q_{ext}|J_g|^2$$

where Q_{ext} is the external quality factor. For validation purposes, $\Delta\omega = 0$ and $\phi_b = \pi/2$, so this expression, using Equation 1, simplifies to:

$$P_g(x) = \frac{1}{2}(R/Q)_\perp Q_{ext}\left[\frac{V_\perp}{2(R/Q)_\perp}\frac{1}{Q_L} + \frac{x\omega}{c}\cdot I_{b,DC}F_b\right]^2 \tag{2}$$

For a given value of x, the power output of the klystron is minimized at some optimal value of Q_L. Assuming $Q_0 >> Q_{ext}$ and thus $Q_L \approx Q_{ext}$, the optimal external quality factor is given by [4]:

$$Q_{ext,opt} = \frac{c}{\omega x}\cdot\frac{V_\perp}{2(R/Q)_\perp I_{b,DC}F_b}$$

Figure 26 shows these analytical expressions together with simulation results for three different values of x_{error}.

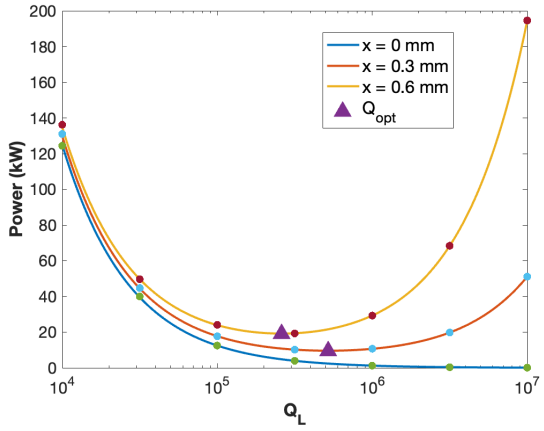

Figure 26: Mean transmitter power vs Q_L.

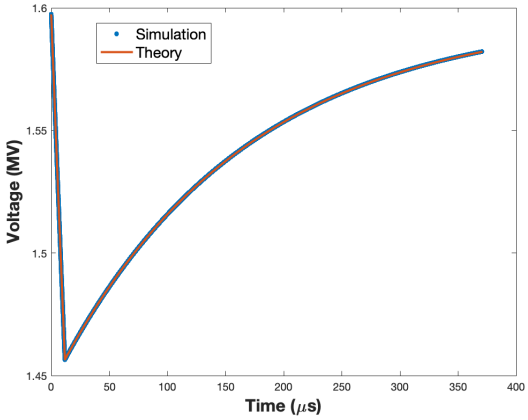

Figure 27: Crab Cavity voltage transient after single bunch train passage.

There is clearly very good agreement between simulation results and analytical expressions. Observe that the optimal Q_l matches indistinguishably with the minimum of the power curve, as expected. In the $x = 0$ case, the curve does not have a minimum and the optimal Q_l is ∞.

We then use the induced voltage in the crab cavities after a beam step to validate the simulation's *transient* response. A *continuous* beam passing through the crab cavity will induce a voltage given by

$$V_{ind} = I_{peak}F_b(R/Q)_t Q_L\frac{x\omega}{c}e^{-j\phi_b} \tag{3}$$

where I_{peak} is the peak beam current. As a result,

$$V_{cav}(t) = V_0 + V_{ind} - V_{ind}e^{-t/\tau} \tag{4}$$

where τ is equal to $Q_L/(\pi f_{RF})$. The cavity voltage returns to the nominal value with the same time constant τ. Figure 27 shows the voltage in the cavity induced by the arrival of a *continuous* beam. The simulated data points are overlaid onto the induced voltage analytical expression from Equations 3 and 4. There is again excellent agreement between simulation and analytical expression.

There might be an opportunity for further simulation validation at the Super-Proton Synchrotron (SPS) at CERN, with real machine data.

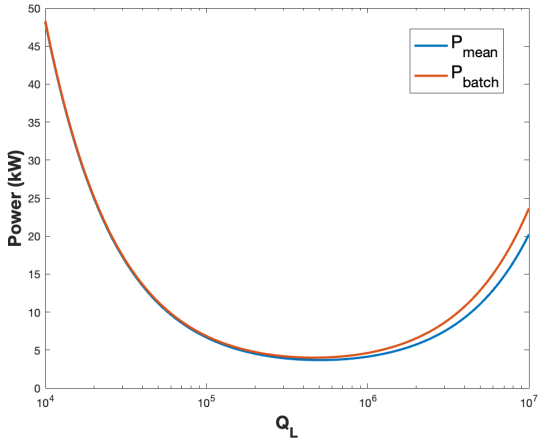

Figure 28: Mean and peak transmitter power as a function of Q_L.

C Power with peak beam current

Equation 2 presents the transmitter power in *steady state*, or equivalently, the mean power corresponding to the DC beam current for a realistic beam pattern. The transmitter power during the bunch train P_{batch} (once the LLRF transients have settled), is instead given by:

$$P_{batch}(x) = \frac{1}{2}(R/Q)_{\perp} Q_{ext} \left[\frac{V_{\perp}}{2(R/Q)_{\perp}} \frac{1}{Q_L} + \frac{x\omega}{c} \cdot \frac{I_{peak}}{2} F_b \right]^2 \tag{5}$$

where $I_{peak} = 2 * N_p * q / T_b$ is the RF component of the peak current, with q the particle charge, and T_b the bunch spacing.

As a result, P_{batch} and the mean transmitter power P_{mean} in the absence of transients are optimized for different Q_L values for a given x_{error}. Figure 28 shows P_{batch} and P_{mean} as a function of Q_L for various values of x_{error} (without transients). Since the EIC gap is small, there is not much of a difference between P_{batch} and P_{mean}. It should be noted that the actual peak power will be higher than both of these values due to the transient response.

D OTFB Lowpass filter bandwidth

The OTFB path includes a lowpass filter (LPF). Since the cavity cannot respond past the closed-loop bandwidth (≈650 kHz for a delay of 320 ns), any signal injected at the input of the transmitter by the RF Feedback and OTFB at higher frequencies leads to unnecessary modulation of the transmitter power. The OTFB LPF will reduce these perturbations and any noise from the cavity antenna and RF demodulator.

The ideal setting for this filter is not evident though. It should be higher than the closed loop bandwidth to avoid loop stability issues, but the exact value is not obvious. Figures 29-32 show the system performance (transverse offsets) and transmitter power for four settings of the filter's 3 dB bandwidth (f_{3dB}). Clearly, the highest setting has the best performance *and* the lowest power transients. We should note though that the simulation does not include noise sources, so there might be some *very* small amplification of noise in the real system.

Given these results, a 3dB bandwidth in the range of 1 to 1.2 MHz seems optimal.

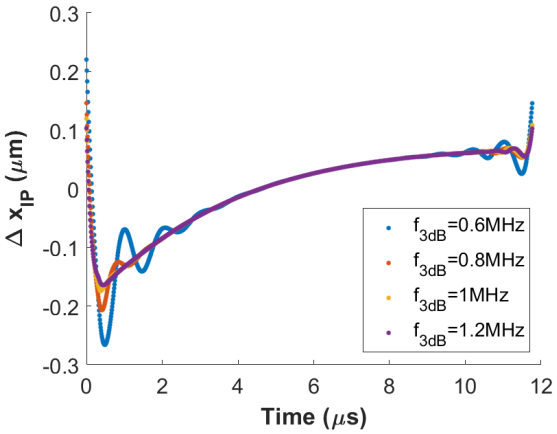

Figure 29: x-offset at the IP.

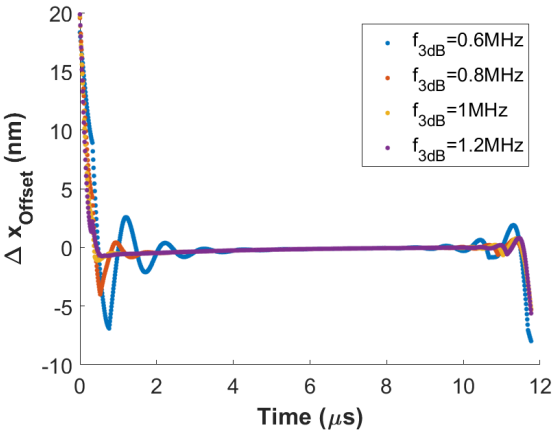

Figure 30: Residual x-offset after uncrabbing.

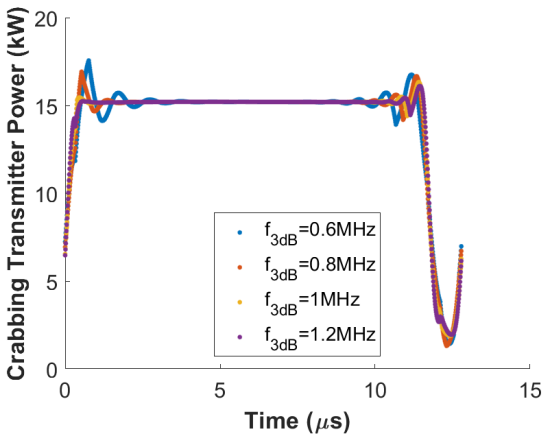

Figure 31: Crabbing transmitter power.

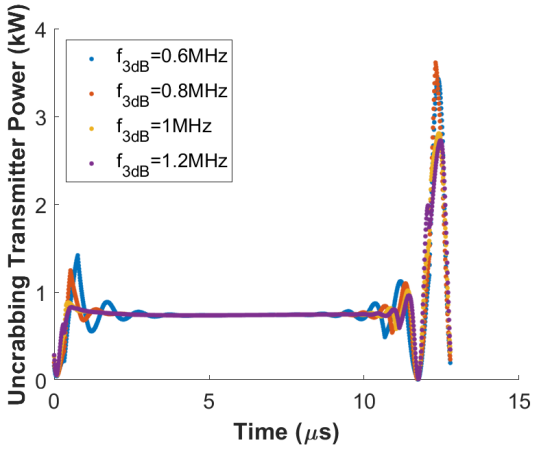

Figure 32: Uncrabbing transmitter power.